Korean J. Chem. Eng., **26**(2), 592-602 (2009)

Reactivity of a $CaSO_4$-oxygen carrier in chemical-looping combustion of methane in a fixed bed reactor

Qilei Song†, Rui Xiao, Zhongyi Deng, Laihong Shen, and Mingyao Zhang

Thermoenergy Engineering Research Institute, School of Energy and Environment,
Southeast University, Nanjing 210096, China
(*Received 1 August 2008 • accepted 15 October 2008*)

Abstract−Chemical-looping combustion (CLC) is a promising technology for the combustion of gas or solid fuel with efficient use of energy and inherent separation of CO_2. A reactivity study of $CaSO_4$ oxygen carrier in CLC of methane was conducted in a laboratory scale fixed bed reactor. The oxygen carrier particles were exposed in six cycles of alternating reduction methane and oxidation air. A majority of CH_4 reacted with $CaSO_4$ to form CO_2 and H_2O. The oxidation was incomplete, possibly due to the $CaSO_4$ product layer. The reactivity of $CaSO_4$ oxygen carrier increased for the initial cycles but slightly decreased after four cycles. The product gas yields of CO_2, CH_4, and CO with cycles were analyzed. Carbon deposition during the reduction period was confirmed with the combustible gas ($CO+H_2$) in the product gas and slight CO_2 formed during the early stage of oxidation. The mechanism of carbon deposition and effect was also discussed. SO_2 release behavior during reduction and oxidation was investigated, and the possible formation mechanism and mitigation method was discussed. The oxygen carrier conversion after the reduction decreased gradually in the cyclic test while it could not restore its oxygen capacity after the oxidation. The mass-based reaction rates during the reduction and oxidation also demonstrated the variation of reactivity of $CaSO_4$ oxygen carrier. XRD analysis illustrated the phase change of $CaSO_4$ oxygen carrier. CaS was the main reduction product, while a slight amount of CaO also formed in the cyclic test. ESEM analysis demonstrated the surface change of particles during the cyclic test. The reacted particles tested in the fixed bed reactor were not uniform in porosity. EDS analysis demonstrated the transfer of oxygen from $CaSO_4$ to fuel gas while leaving CaS as the dominant reduced product. The results show that $CaSO_4$ oxygen carrier may be an interesting candidate for oxygen carrier in CLC.

Key words: Chemical-looping Combustion, $CaSO_4$ Oxygen Carrier, Reactivity Study, Methane, Fixed Bed

INTRODUCTION

Chemical-looping combustion (CLC) has been proposed as a new technology that can be used to control the greenhouse gas emission with less energy loss [1]. A CLC system consists of two interconnected reactors, the fuel and the air reactor. The oxygen is transferred by the solid oxygen carrier from the air to the fuel. The water in combustion products can be easily removed by condensation, and pure carbon dioxide is obtained without any loss of energy for separation.

The development of oxygen carrier is a key technology in CLC. A number of metal oxides have been extensively investigated as potential oxygen carriers in CLC of methane or natural gas in many research centers such as the Tokyo Institute of Technology [2,3], Chalmers University of Technology in Sweden [4-7], CSIC [8-11], Korea Institute of Energy Research [12-15] and Korea Advanced Institute of Science and Technology [16,17], and Southeast University [18-20] in China. Overall, the general conclusion of these studies on oxygen carrier development is that metal oxide oxygen carriers demonstrate high reactivity and Nickel-based oxygen carrier shows the highest among these metal oxides. However, these oxygen carriers also have some significant disadvantages for applications in the CLC system: high cost of these metal materials, the heavy carbon deposition problem, and potential heavy-metal pollution to the environment.

As a novel oxygen carrier, $CaSO_4$ has many advantages. It is much more environmentally sound as a nonmetal oxide. $CaSO_4$ is cheaper due to vast gypsum resources all over the world. Compared with metal oxides, $CaSO_4$ has a relatively higher oxygen capacity. The oxygen ratio shows the maximum amount of oxygen that can be transferred between the air and fuel reactors. The theoretical value of R_O for $CaSO_4$/CaS is 0.4706, which is much higher than that of many other metal oxides [21].

Alstom Power Inc. have started investigation on the feasibility of $CaSO_4$ based oxygen carrier in CLC system [22], but they still have not published key data yet. CANMET has explored the use of $CaSO_4$ as oxygen carrier in a process for gasification of solid fuels and following the CLC process [23,24]. In our previous studies, the feasibility of $CaSO_4$ oxygen carrier was investigated through thermodynamic analysis and thermogravimetric analysis with Fourier transform infrared spectroscopy [19]. The results show that $CaSO_4$/CaS can be an interesting alternative oxygen carrier for the CLC system. A reduction test of $CaSO_4$ oxygen carrier with methane in CLC has been investigated in a fixed bed reactor, The results showed that $CaSO_4$ oxygen carrier has a high reduction reactivity and regenerability in a long-time reduction/oxidation test [25]. However, cyclic tests of reduction and oxidation are necessary to further investigate the reactivity of $CaSO_4$ oxygen carrier.

A CLC system using two interconnected fluidized bed reactors

†To whom correspondence should be addressed.
E-mail: qlsong@seu.edu.cn
‡This work was presented at the 7th China-Korea Workshop on Clean Energy Technology held at Taiyuan, China, June 26-28, 2008.

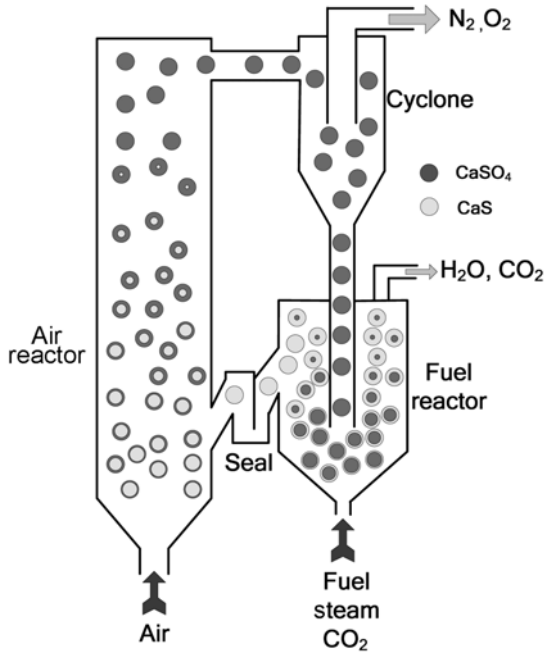

Fig. 1. Concept of chemical-looping combustion with two interconnected fluidized bed reactors.

is shown in Fig. 1. This CLC system is proposed for direct use of coal and other solid fuels such as biomass, solid wastes and cokes [18]. It is mainly composed of a bubbling fluidized bed, a high velocity fluidized bed, a cyclone and the oxygen carrier. The solid fuels need to be gasified in the bubbling fluidized bed by H_2O or CO_2 to produce syngas first, and then the syngas reacts with the oxygen carrier.

$CaSO_4$ is reduced by natural gas (CH_4) or syngas ($CO+H_2$) to calcium sulfide (CaS) in the fuel reactor:

$$CaSO_4+CH_4 \rightarrow CaS+CO_2+2H_2O \qquad \Delta H^{\theta}_{298\,K}=158.61\ kJ/mol \qquad (1)$$

$$CaSO_4+4CO \rightarrow CaS+4CO_2 \qquad \Delta H^{\theta}_{298\,K}=-170.96\ kJ/mol \qquad (2)$$

$$CaSO_4+4H_2 \rightarrow CaS+4H_2O \qquad \Delta H^{\theta}_{298\,K}=-6.41\ kJ/mol \qquad (3)$$

Then CaS is transported to the air reactor to be oxidized back to $CaSO_4$:

$$CaS+2O_2 \rightarrow CaSO_4 \qquad \Delta H^{\theta}_{298\,K}=-960.90\ kJ/mol \qquad (4)$$

This cycle can transfer the oxygen from the air to the fuel, and the carbon dioxide is obtained in almost pure form without extra energy input.

Since solid fuel gasification technology has been extensively investigated and proved to be mature [26-28], during the process of coal gasification, CH_4, other hydrocarbons, CO, and H_2 are the main products which are all important intermediates in CLC of solid fuels. It is of practical interest to investigate the reactivity of oxygen carrier with these gaseous intermediates for the development of a solid fueled CLC system. It would also be important to investigate the reactivity of $CaSO_4$ in CLC of natural gas.

The main purpose of this study was to investigate the reactivity of $CaSO_4$ oxygen carrier in CLC of methane. Six cycles of alternating reduction and oxidation were performed in the fixed bed.

Table 1. Material properties

Producing area	Nanjing, China
particle size, mm	0.15-0.2
specific density, kg/m^3	2900
bulk density, kg/m^3	1500
BET surface area, m^2/g	0.5266
Chemical composition, %	
$CaSO_4$	94.380%
MgO	1.680
SiO_2	0.630
Fe_2O_3	0.094
Al_2O_3	0.120
TiO_2	0.014
K_2O	0.044
Na_2O	0.055
P_2O_5	0.028
Crystallization water	2.955

The gas concentrations with time were obtained. The release of sulfur in the oxygen carrier was also investigated. The carbon yield and deposition were also discussed. The oxygen carrier conversion and mass-based reaction rates during reduction and oxidation were investigated. A series of characterization analyses were performed to investigate the reaction mechanism.

EXPERIMENTAL

1. Material Preparation and Characterization

The oxygen carrier particle used was natural anhydrite ore from Nanjing Anhydrite Ore Co. Ltd. $CaSO_4$ is the main content in natural anhydrite ore (94.38%). The specific information is presented in Table 1.

The fresh and used oxygen carriers were characterized by X-ray diffraction (XRD) for their crystal structure in a D/max 2500VL/PC system by using Cu Kα radiation with a step of 0.02° per second. The morphology of the fresh and used oxygen carriers was recorded by environmental scanning electron microscope (ESEM) in a microscope system (QUANTA 200, FEI, Holland) equipped with an energy-dispersive X-ray spectroscopy (EDS) system (INCA X-sight, OXFORD INSTRUMENTS, Britain).

2. Experimental Setup

The experiment was conducted in a bench-scale fixed bed reactor under atmospheric pressure. The schematic diagram of the fluidized bed reactor is shown in Fig. 2.

The stainless steel tube reactor (internal diameter=25 mm, height=950 mm) tube with 480 mm of heating zone above the porous plate is electrically heated in the furnace. The reaction temperature was controlled by a temperature controller with a Pt/Rh thermocouple between the tube and the heater. Another K-type thermocouple inside the tube was adjustable along the bed height to monitor the reaction temperature in the reactor. The feeding gases were CH_4, nitrogen, and air and measured by three mass flow controllers. The pressure difference (ΔP) of the fixed bed was measured by a pressure gauge. The gas produced from the reactor was sent to an ice-water cooler where the steam was condensed and removed. The dry prod-

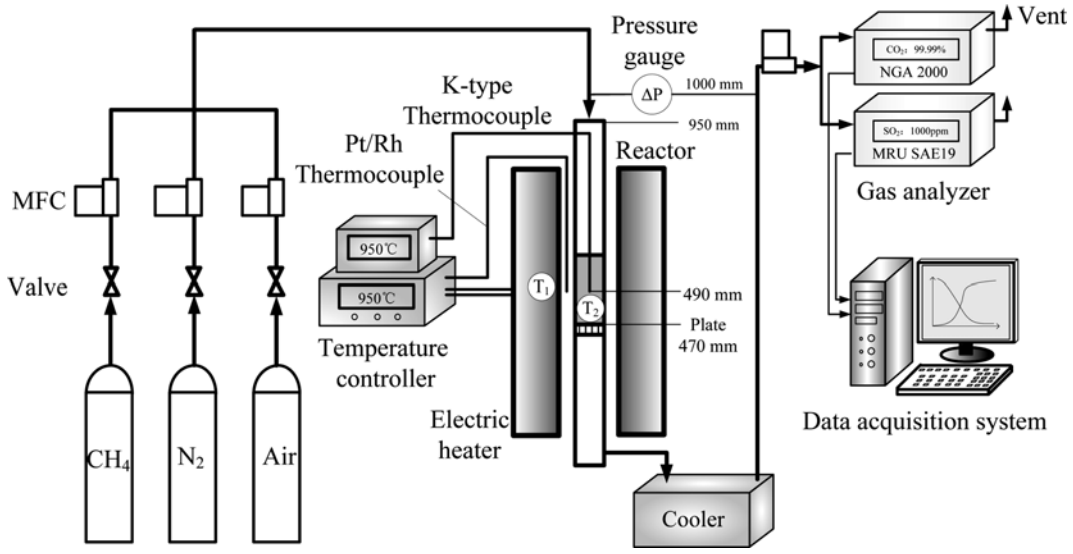

Fig. 2. Schematic diagram of the experimental setup.

uct gas flow rates were measured by two mass flow meters, one for reduction test and one for the oxidation period. Then the product gas was sent to the gas analyzers. The product gas concentrations were measured by two online gas analyzers. One stream of gas was measured by an MRU SAE19 flue gas analyzer to detect the dry concentration of O_2, SO_2, H_2S and NO_X. The other gas stream was sent to Emerson multicomponent gas analyzers including a Rosemount NGA 2000 gas analyzer used to measure the concentrations of CO_2, CH_4, CO, and O_2, and a Hydros 100 analyzer to detect the concentration of H_2.

It should be noted that because of the long gas residence time in the reactor and the time delay from the reactor inlet to the gas analyzers, the gas concentrations that were obtained reached to the gas analyzers instead of the real-time gas concentration in the reactor. So for the gas component in the product gas, the backmixing in the system should be considered; N_2 accounts for a large part in the early period which is not displayed in this study. In our recent work this reactor system has been adapted to a fluidized bed and the gas hold-up time was largely shortened.

3. Experimental Procedure

The fresh oxygen carrier was added into the reactor on the porous plate. The K-type thermocouple was adjusted in the middle of the particles. Then oxygen carrier was preheated gradually in the N_2 atmosphere to the desired reaction temperature. Then the reaction gas was introduced to replace pure nitrogen and the reduction started. The concentrations of product gas were measured by the two online gas analyzers.

The operation conditions were determined by reference to our previous study [25]. The suitable reduction temperature for high reactivity and relative low sulfur release seems to be around 950 ºC, so in this study the reduction temperature was set to 950 ºC. It is also found that the reduction time is necessarily to be shortened to avoid significant carbon deposition, which usually occurs during the late period of reduction. Considering the high recirculation rate of oxygen carriers between the two reactors, it is not practical to reduce the oxygen completely as reported in the literature on metal oxide. And due to the limitation of the experimental facilities, the relatively long hold-up time indicates that the reduction duration cannot be too short, or the gas concentration peak may not show. So the reduction gas supply duration was set to 20 min. The inlet methane gas flow rate was 50 mL/min. When the reduction was finished the gas was switched to N_2 (100 mL/min). The data in this stage was also recorded for 10 min until the product gas was cleared away. Then the reactor heater was adjusted with PID controller to an oxidation temperature at 850 ºC. Then the oxygen carrier was exposed to the air and the oxidation started. The inlet oxidizing air flow rate was set to 1,000 mL/min. The oxidation duration was all set to 10 min which was determined considering the fact that the oxidation of CaS was nearly complete after 10 min. Then the gas was switched to N_2 (500 ml/min). When the product gas was blown away, the heater worked to increase the temperature to 950 ºC. Then the next cycle of reduction/oxidation started.

The oxidation temperature requires some explanation. As shown in Eq. (4), the CaS oxidation was a significantly exothermic reaction; a large heat would be generated which could not be removed immediately for the fixed bed reactor in this study. A large temperature increase (as high as 50 ºC) would occur if the oxidation was not controlled, and consequently the bed material would possibly sinter under higher temperatures. Usually, a lower oxygen concentration would be used in the literature. However, for this study the low O_2 concentration might enhance the side reactions which are not expected. Also, there is an optimized temperature scope with less SO_2 release and high conversion of CaS, that is about 840-890 ºC with elevated oxygen partial pressure to the air [29]. So the oxidation temperature was set at 850 ºC and the oxidation rate was decreased at this lower temperature. During the early stage of oxidation in the cyclic test, the temperature increase was within 10 ºC, suggesting the temperature increase was successfully controlled in this study. This method was applied in a previous study [25].

When the cyclic tests were finished, the gas was switched to nitrogen and the heater was shut down. The oxygen carrier particle was cooled in the nitrogen flow to room temperature and collected

Table 2. Experimental conditions

Oxygen carrier	Natural anhydrite ore
Pressure	1 atm
Reaction temperature	950 °C
Sample weight	30 g
Sample height	40 mm
Reduction gas	100% CH_4
Reduction gas flow rate	50 mL/min
Reduction duration	20 min
Oxidation temperature	850 °C
Oxidation gas	air
Oxidation gas flow rate	1,000 mL/min
Oxidation duration	15 min
Inert gas	N_2
Inert gas flow rate	100, 500 mL/min

for further analysis. During the cyclic test, a slight amount of oxygen carrier particles were also sampled for characterization analysis.

The specific operation conditions concerning the cycle tests are shown in Table 2.

4. Data Evaluation

The gas yield of carbon species in the product gas is defined as follows:

$$\gamma_i = \frac{y_{i,out}}{y_{CO_2,out} + y_{CO,out} + y_{CH_4,out}} \times 100\% \quad (5)$$

The conversion of oxygen carrier or degree of oxidation is defined as:

$$X = \frac{m - m_{red}}{m_{ox} - m_{red}} \quad (6)$$

The conversion of the $CaSO_4$ oxygen carrier as a function of time for the reducing period considering the mass balance of oxygen is defined as follows:

$$X_{r,i} = x_{r,i-1} + \int_{i-1}^{t_i} \frac{\dot{n}_{out}}{n_o}(4y_{CO_2,out} + 3y_{CO,out} - y_{H_2,out} + 2y_{SO_2,out})dt \quad (7)$$

Similarly, the following equation is used to calculate oxygen carrier conversion during the oxidation:

$$X_{o,i} = X_{o,i-1} + \int_{i-1}^{t_i} \frac{2}{n_o}\left(\dot{n}_{in}y_{O_2,in} - \dot{n}_{out}\left(y_{O_2,out} + \frac{1}{2}y_{CO,out} + y_{CO_2,out} + y_{SO_2,out}\right)\right)dt \quad (8)$$

A mass-based conversion is used to compare the reactivity of different oxygen carriers in the literature, and defined as follows:

$$\omega = \frac{m}{m_{ox}} = 1 + R_O(X - 1) \quad (9)$$

The mass-based reduction rate was calculated from the reduction and oxidation rate as follows:

$$\frac{d\omega}{dt} = R_O\frac{dX}{dt} \quad (10)$$

More information on the data evaluation can be found in the references [5,7,30-32].

RESULTS AND DISCUSSIONS

1. The Gas Concentration with Time

Fig. 3 shows the product gas concentrations as a function of time during the 3rd cycle of reduction and oxidation. The time started when the inlet gas was switched from N_2 to CH_4. As stated in the Experimental section, the gas holdup time should be considered. During the reduction period in Fig. 3(a), the initial 5-10 min was a period when the inlet fuel gas was purging the N_2. The CH_4 and product gas CO_2 and H_2O still had not reached the reactor. After this purging period, when the nitrogen gas in the reactor was cleaned up by the product gas, the product gas CO_2 and unconverted CH_4 appeared and the concentrations of CO_2 and CH_4 gradually increased. The concentration of CO_2 increased significantly to the peak value

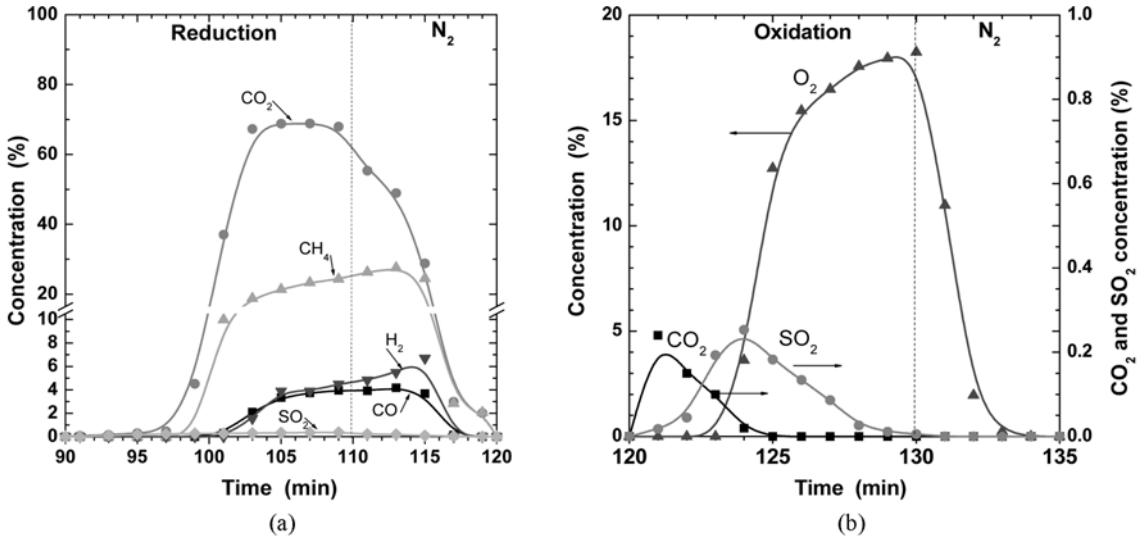

Fig. 3. Product gas concentrations for $CaSO_4$ oxygen carrier during (a) reduction and (b) oxidation period of the 3rd cycle. The dashed lines indicated the switch to inert atmosphere.

around 70.0%. After CO_2 had surmounted its peak value and remained stable for about 5 min, it began to decrease while the CH_4 concentration increased and reached the peak value of 27.6% after the switch of CH_4 to N_2. As the reaction proceeded, more unconverted CH_4 was released. Also there was formation of some minor amounts of CO and H_2 at the later period. Slight amount of SO_2 was also observed during the reduction period, which will be discussed in the SO_2 formation and mitigation section. After the switching of CH_4 to N_2, the product gas was cleared up within 10 min. Overall, it can be claimed that a majority of CH_4 was converted to CO_2 and H_2O during the reduction.

Fig. 3(b) shows the gas concentrations during the oxidation period. The time started when the temperature was stable and oxidizing air was introduced. The time delay was shortened in this period because of the high inlet gas flow rate. O_2 was not observed during the first 3 min. This indicated that the reaction rate was initially quite fast and the rapid conversion was obtained at the early stage. Then the reaction slowed down with most of the O_2 being released without reacting. At the end of the oxidation period, the concentration of oxygen increased to 18.24%, which indicated that the conversion of CaS to $CaSO_4$ was incomplete. Many investigations showed that the incomplete oxidation was due to the $CaSO_4$ product layer that increased the intraparticle diffusion resistance to oxygen and prevented the complete oxidation [33,34]. Besides, at the early stages of oxidation, there were slight CO_2 and SO_2 observed, which will be discussed later.

Fig. 4 shows the product gas concentrations during the six cycles. The N_2 purging period is included in the reduction and oxidation periods and not displayed. The temperature adjustment period was also not displayed. The majority of inlet methane reacted with the $CaSO_4$ oxygen carrier to form CO_2 and H_2O. The reactivity varied as indicated from the variation of CO_2 peak and CH_4 peak. The CO_2 concentration was around 60% at the first cycle and then increased to the maximum value of 77.6% at the 4th cycle. However, CO_2 seems to decrease after the 4^{th} cycle. The CH_4 concentration varied accordingly. The variation of gas concentration demonstrated that the reactivity of $CaSO_4$ oxygen carrier increased for the initial cycles but slightly decreased after four cycles.

The initial increase of CO_2 concentration may be possibly due to the particle structure change as discussed later. The particles became much more porous on the surface, which facilitated the diffusion of reactant gas to the reaction film. Therefore, the reduction reaction can proceed further to the kernel in the cyclic test. However, during the cyclic test, there was also a certain amount of sulfur release from the $CaSO_4$ oxygen carrier, which means the irreversible loss of oxygen capacity. The decrease of oxygen capacity is also demonstrated in the oxygen carrier conversion section. The reduction degree increased, but the oxidation conversion could not restore to the original oxygen capacity. Therefore, the CO_2 concentration decrease may be explained by the release of sulfur and oxygen from the oxygen carrier.

2. Carbon Yield and Deposition Route

As presented above, the variation of product gas concentrations versus time is compared. In this section, the variation of total product gas yield (dry basis) with cycles is presented, which would be much more evident to compare the gas conversion with cycles. The yield of carbon in the product gas is calculated from the integration of amounts of CH_4, CO_2, and CO divided by the total amount of inlet carbon. As shown in Fig. 5, the yield of CO_2 gradually increased for the initial cycles and then slightly decreased. In contrast, the yield of CH_4 displayed a different trend. The variation is in accordance with the product gas concentration. Therefore, the yield of carbon species reflects the variation of $CaSO_4$ reactivity during the cyclic test of reduction and oxidation.

The gas yield of CO also provides information for the side reac-

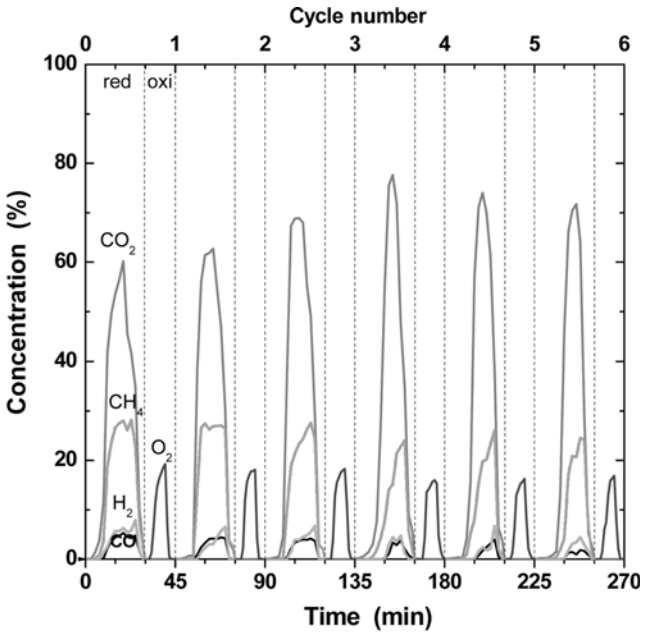

Fig. 4. The product gas concentrations as a function of time during the six cycles. The time started when the reaction gas was introduced. The dashed lines indicate the switch of reduction and oxidation atmosphere.

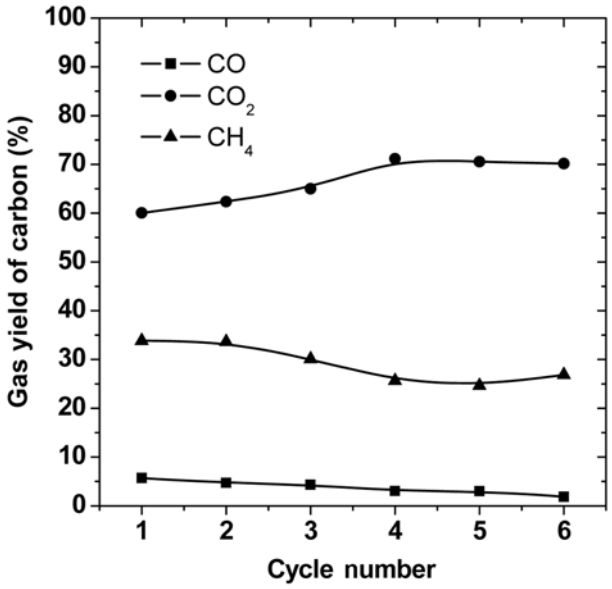

Fig. 5. The average gas yield of CH_4, CO and CO_2 in the product gas as a function of cycle number during the six-cycle test.

tions. Previous studies have investigated the carbon formation on nickel-based oxygen carrier particles for CLC of methane and coal gas [12,15,35-38]. Generally, the formation of CO and H_2 yields to the thermodynamic limitations of $CaSO_4$, which is similar to the metal oxide oxygen carrier. When the amount of oxygen provided to oxidize the CH_4 was sufficient, the product would be CO_2 and H_2O and the carbon formation was negligible. However, when the oxygen to CH_4 was less than the stoichiometry ratio or large amount of oxygen had been transferred, CO and H_2 would form and carbon deposition would occur. Previous work has successfully demonstrated that significant carbon deposition occurred at the later reduction period when the oxygen carrier was nearly completed [25]. As presented in our previous study, carbon formation was mainly through catalytic methane decomposition as follows:

$$CH_4 \rightarrow C+H_2 \qquad \Delta H^{\theta}_{298\,K}=86.3\ \text{kJ/mol} \qquad (11)$$

The small amount of carbon formed during the reduction was also reflected by the CO yield. As presented in the literature [35], carbon is possibly a reaction intermediate of CH_4 oxidation. The related reactions were also possible:

$$C+CO_2 \rightarrow 2CO \qquad \Delta H^{\theta}_{298\,K}=172.4\ \text{kJ/mol} \qquad (12)$$

$$C+H_2O \rightarrow CO+H_2 \qquad \Delta H^{\theta}_{298\,K}=131.3\ \text{kJ/mol} \qquad (13)$$

Under the operation conditions in this study, because the methane was introduced continuously and the residence time of product gas in the fixed bed was relatively longer, therefore, the methane reforming may also be possible:

$$CH_4+H_2O \rightarrow CO+3H_2 \qquad \Delta H^{\theta}_{298\,K}=205.0\ \text{kJ/mol} \qquad (14)$$

$$CH_4+CO_2 \rightarrow 2CO+2H_2 \qquad \Delta H^{\theta}_{298\,K}=247.1\ \text{kJ/mol} \qquad (15)$$

According to our previous study on methane reforming mechanism [39], reactions (14) and (15) could possibly be composed of reactions (11)-(13). So this may suggest that reaction (11) was the main reaction.

The deposited carbon on the surface of oxygen carrier could also possibly react with $CaSO_4$ via following solid-solid reaction even though it may be difficult for this reaction to proceed.

$$CaSO_4+4C \rightarrow CaS+4CO \qquad \Delta H^{\theta}_{298\,K}=518.7\ \text{kJ/mol} \qquad (16)$$

The CO and H_2 formed through the above reactions would be converted to CO_2 and H_2O through reactions (2) and (3).

The CO fraction was quite low and decreased to around 1.8% at the sixth cycle. Also during the early stage of oxidation, there were lower concentrations of CO and CO_2 detected (<0.2%) in the product gas, which is negligible to observe in Fig. 3(b). These data indicate the degree of carbon deposition during the reduction was negligible. In previous studies, the extent of carbon formation was much lower with abundant oxygen carrier provided. The carbon deposition problem was once considered a problem for oxygen carrier deactivation. However, recent studies show that the carbon deposition may not be a problem for CLC if abundant oxygen carrier is provided [24]. According to the latest findings, unconverted CH_4 and combustible CO and H_2 in the product gas from a fuel reactor could be oxidized immediately after the cyclone by adding a stream of oxygen, which is called "oxygen polishing process" [40]. This process may need extra energy and cost but a high gas conversion could be attained.

3. SO_2 Formation and Mitigation

The release of SO_2 involved with $CaSO_4$ and CaS is varied with the operating conditions as illustrated in many investigations [41-44]. SO_2 formation is mainly due to the solid-solid reactions and also the partial oxidation at the initial oxidation period:

$$CaS+3CaSO_4 \rightarrow 4CaO+4SO_2 \qquad \Delta H^{\theta}_{298\,K}=1047.9\ \text{kJ/mol} \qquad (17)$$

$$CaS+3/2O_2 \rightarrow CaO+SO_2 \qquad \Delta H^{\theta}_{298\,K}=-458.7\ \text{kJ/mol} \qquad (18)$$

Side reactions during the reduction period were also possible:

$$4CaSO_4+CH_4 \rightarrow 4CaO+CO_2+4SO_2+2H_2O \qquad \Delta H^{\theta}_{298\,K}=1206.5\ \text{kJ/mol} \qquad (19)$$

As presented in the literature by Anthony [45] and Mattisson and Lyngfelt [46], $CaSO_4$ is a thermodynamically stable product at typical FBC temperatures (800-950 °C) and the overall oxidizing conditions. CaS is a stable product at strongly reducing conditions, while $CaSO_4$ is a stable compound at highly oxidized conditions. CaO is favored thermodynamically in intermediate conditions, which can be expected during the shifts between oxidizing and reducing conditions.

Fig. 6 shows the variation of SO_2 concentration in the dry product gas as a function of time during the cyclic test of reduction and oxidation. The N_2 purging period is included in the reduction and oxidation periods and not displayed. It is clear that the SO_2 concentration increased for the initial cycles of reduction and oxidation and gradually decreased after the 4th cycle, and H_2S was not observed in this study. As illustrated above, the variation of SO_2 release with cycles may also be explained by the side reactions in the cyclic test, including the competing reduction, solid-solid reaction and partial oxidation. Because the reduction degree increased during the initial three cycles, the CaS product content also increased accordingly. Therefore, the contact between CaS and $CaSO_4$ was enhanced and,

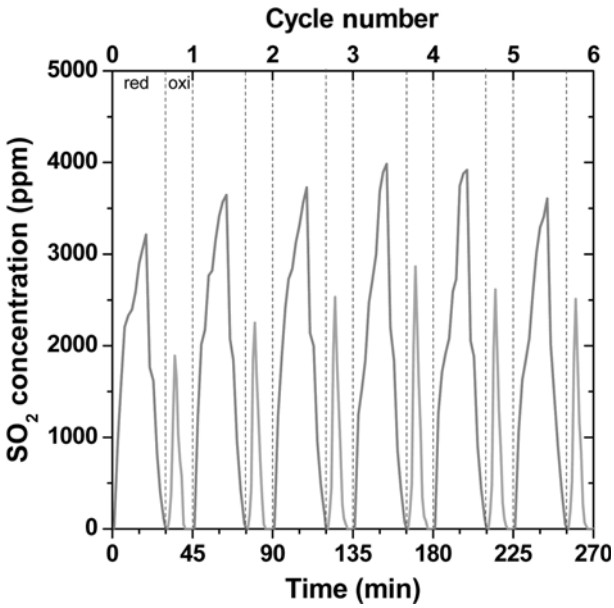

Fig. 6. The outlet SO_2 concentration as a function of time during the cyclic tests. The dashed lines indicate the switch of reduction and oxidation atmosphere.

consequently, the SO_2 release increased during the initial cycles. Also, the side reaction 19 might also be promoted with the particle structure change. Consequently, the SO_2 release during the early cycles caused the decrease of oxygen capacity. As a result, the SO_2 emission slightly decreased at the later cycles.

Even though certain measures were undertaken to control the oxidation temperature increase, a considerable amount of SO_2 was released during the oxidation period. During the early stage of oxidation, reactions (4) and (18) were both strongly exothermic. The temperature increased by as high as 10 °C in some cycles during the early stages and soon decreased to 850 °C. Reactions (17) and (19) are endothermic and would be enhanced with the temperature increased. The oxidation might be promoted if fluidization condition was adopted, which should be paid attention in further study.

The sulfur release is involved with complicated reactions, so it may become a key limitation for the use of $CaSO_4$ oxygen carrier in CLC. In our recent published article, a possible solution to sulfur release was proposed [19]. As presented by Shen et al., although certain amount of SO_2 was released during the process of CLC using a $CaSO_4$ based oxygen carrier during the reactions of CaS oxidization and $CaSO_4$ reduction, it can be recaptured by adding a small amount of fresh limestone into the system of CLC, and the products of $CaSO_4$ and CaS can be used as oxygen carriers later. The sulfur mitigation method for $CaSO_4$ oxygen carrier in CLC of solid fuels is described as follows.

Fresh limestone and CaO sorbent particles are fed with coal into the fuel reactor and reast via the following reactions.

$$CaCO_3 \rightarrow CaO+CO_2 \quad (20)$$

$$CaO+H_2S \rightarrow CaS+H_2O \quad (21)$$

$$CaCO_3+H_2S \rightarrow CaS+H_2O+CO_2 \quad (22)$$

$$CaO+SO_2 \rightarrow CaSO_3 \quad (23)$$

The oxygen carrier particles, desulfurization products (CaS, $CaSO_3$), and unreacted CaO are all transported to the air reactor and expected to be oxidized to $CaSO_4$. The SO_2 emission in the air reactor may also be captured with the unreacted CaO.

$$CaO+SO_2+1/2O_2 \rightarrow CaSO_4 \quad (24)$$

The desulfurization product may also serve as oxygen carrier. Therefore, the additional costs for sulfur capture including capital, operation and maintenance might be reduced greatly. However, further work is essential to test the effect of CaO on the sulfur reduction. And it is still a long way for commercial use of this process.

4. The Oxygen Carrier Conversion Versus Cycles

The oxygen carrier conversion or the degree of oxidation during the six cycles of reduction/oxidation test is shown in Fig. 7. It is evident that the oxygen carrier conversion after the reduction reaction decreased gradually in the cyclic test. The decrease of conversion after each reduction period indicates the increase of extent of reduction, and more oxygen in the oxygen carrier was utilized with the number of cycles. This trend is in accordance with the gas concentration. It was also observed after each run of oxidation that the

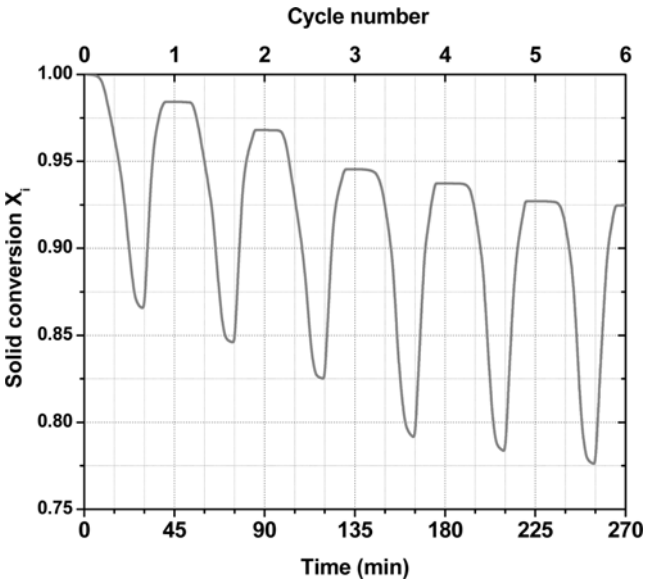

Fig. 7. Variation of oxygen carrier conversion as a function of number of cycles.

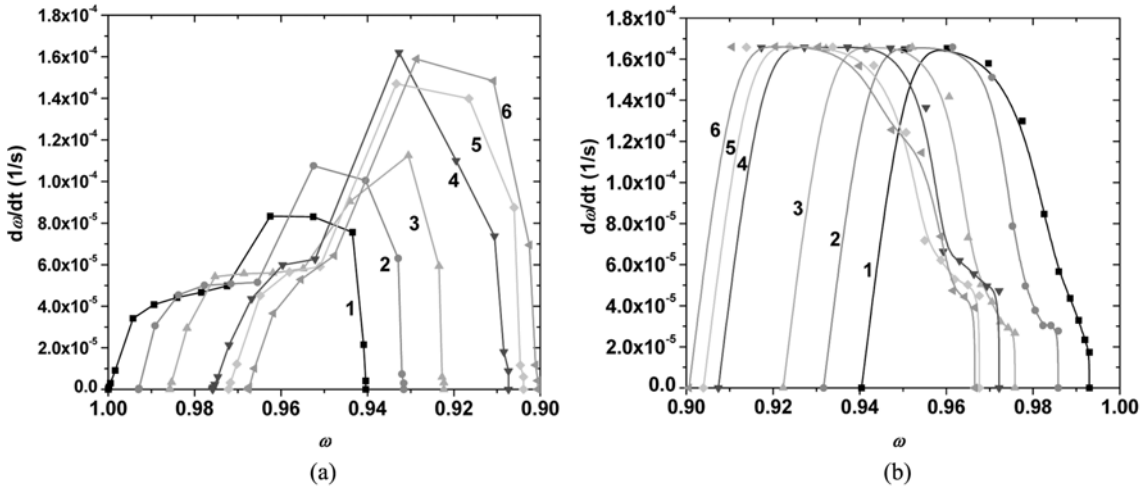

Fig. 8. The mass-based rate dω/dt, as a function of ω for (a) the reduction and (b) the oxidation at typical cycles.

oxygen carrier conversion could not be restored to the same level as that before reduction. This was ascribed to the release of sulfur species during the cyclic test of reduction and oxidation, as discussed in the sulfur formation and mitigation section. There was less oxygen available for reaction with fuel gas and, consequently, resulted in the change in conversion.

Fig. 8(a)-(b) show mass-based reaction rates ($d\omega/dt$) as a function of mass-based degree of conversion (ω) during the reduction and oxidation. As shown in Fig. 8(a), the variation of reaction rate is similar to the previous investigations on methane combustion using metal oxide as oxygen carrier but much lower than metal oxide oxygen carriers [4,47]. The maximum value of mass-based conversion rate is very stable around 1.6×10^{-4} s^{-1}, which is considerably lower than that of Fe_2O_3-based oxygen carrier in the literature [4]. The reduction rate increased for the initial cycles and then became stable, which is in agreement with the gas concentration in Fig. 4 and sulfur release trend in Fig. 6. The mass conversion (ω) decreased significantly after each cycle. As shown in Fig. 8(b), the comparison of mass-based conversion rate as a function of mass conversion for the oxidation period is also evident. It is clear that the reaction rate was relatively higher at the early stages of oxidation. This is attributed to the chemical reaction control at the early stage. It was also demonstrated that the oxidation conversion could not be restored to the original oxygen capacity. The oxidation rate increased for the next few cycles and finally decreased significantly at the end of cycles, suggesting a decrease of oxygen capacity. The time needed for complete oxidation was determined by the extent of reduction. Take the 4^{th} cycle for example, because the extent of 4^{th} reduction was much higher, therefore the initial O_2 conversion was the highest for the 4^{th} oxidation. The incomplete oxidation might be improved by increasing the oxidation temperature. But at higher temperatures the side reactions would also be enhanced.

5. Phase Characterization

The results of XRD analysis of fresh and reacted $CaSO_4$ oxygen carrier of different cycle are shown in Fig. 9. The presence of anhydrite ($CaSO_4$) as the main crystalline phase in the fresh oxygen carrier is clearly evidenced. Fig. 9(b) shows the powder XRD pattern of sample after the reduction stage in the 1^{st} cycle. Clearly, the $CaSO_4$ was still the main component. The presence and intensity of CaS suggests the reduction sulfur species was mainly CaS, which is in accordance with the result of gas conversion. Fig. 9(c) indicates the $CaSO_4$ oxygen carrier can be oxidized back to $CaSO_4$ rather than CaO. However, the intensity of CaO was still observed as demonstrated in SO_2 release during the cycles.

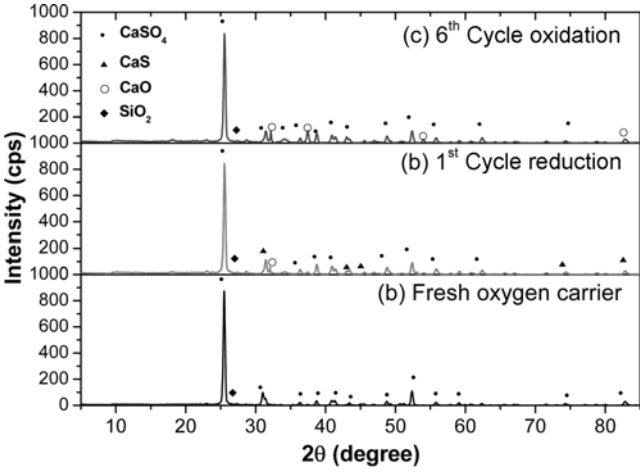

Fig. 9. XRD patterns of $CaSO_4$ oxygen carrier. (a) Fresh, (b) Used after the 1^{st} cycle reduction and (c) Used after the 6^{th} cycle oxidation.

6. ESEM-EDS Analysis of Oxygen Carriers

Figs. 10(a) and 10(b) show the surface morphology of oxygen carrier particle before reduction, which displays that the fresh oxygen carrier is impervious. After one cycle reduction at 900 °C as shown in Figs. 10(c) and 10(d), the surface of the reduced oxygen carrier appears much rougher and more porous. However, the porosity seems not so uniform. This might be ascribed to the gas-solid contact in the fixed bed reactor. While for particles after the 6^{th} cycle oxidation as shown in Figs. 10(e) and 10(f), the appearance of the surface is considerably different from that shown in Figs. 10(c) and 10(d). It seems that the crystal grains on the surface of the particles after six cycles displayed a compact agglomerated state. This result was possibly due to cyclic test of reduction and oxidation and side reactions, especially the high temperature effect [48,49].

The EDS analysis spectrum and average accurate quantitative analysis of atomic percentage of major elements are shown in Fig. 11 and Table 3, respectively. At each spectrum shown in Fig. 11(a)-(c), there is slight peak of Mg observed that is in agreement with the chemical component, which would not have an obvious effect on the reaction.

The average quantitative value of O/Ca and S/Ca of fresh and used oxygen carrier particles was obtained. The variation of O/Ca and S/Ca may indicate the transfer of oxygen can sulfur on the surface based on the fact that the content of Ca in the particle was constant during the cyclic test. For the fresh $CaSO_4$ particles shown in Fig. 10(b), the S and Ca peaks were comparable in Fig. 11(a). The S/Ca ratio was 1.146 and the O/Ca ratio was 4.211, which verified the main component of $CaSO_4$ in the particles. This result is in agreement with the literature, that is, the S/Ca ratio of 1.1 is expected for both CaS and $CaSO_4$ [50].

As for the first cycle reduction, the EDS analysis was focused on the porous area shown in Fig. 10(d). The intensity of O decreased significantly with the O/Ca ratio decreased to 0.0026, while the S is still comparable to Ca peak with S/Ca around 1.0972 in Fig. 11(b). This spectrum successfully demonstrates the process of oxygen transfer from the oxygen carrier to the fuel gas to CO_2 and H_2O, and CaS is the dominant product. For the typical particles shown in Fig. 10(f), S/Ca and O/Ca ratio on the surface decreased to 0.836 and 3.635 after six cycles, respectively. The considerable decrease indicated the loss of sulfur and oxygen compared to the fresh oxygen carrier. This loss was irreversible and accounted for the decrease of oxygen carrier ability to transport oxygen. The results of ESEM-EDS study verified the variation of reactivity of $CaSO_4$ oxygen carrier.

The above characterization analyses also provide information concerning the reaction mechanisms. During the reduction of $CaSO_4$, CH_4 gradually diffuses to the $CaSO_4$ core through the film surrounding the particle, and reacts with the $CaSO_4$ on the surface to form mainly H_2O and CO_2 and CaS solid product. A certain amount of CaO and SO_2 is also formed due to the side reactions. As presented above, the outer product layer is mainly CaS and the inner core is

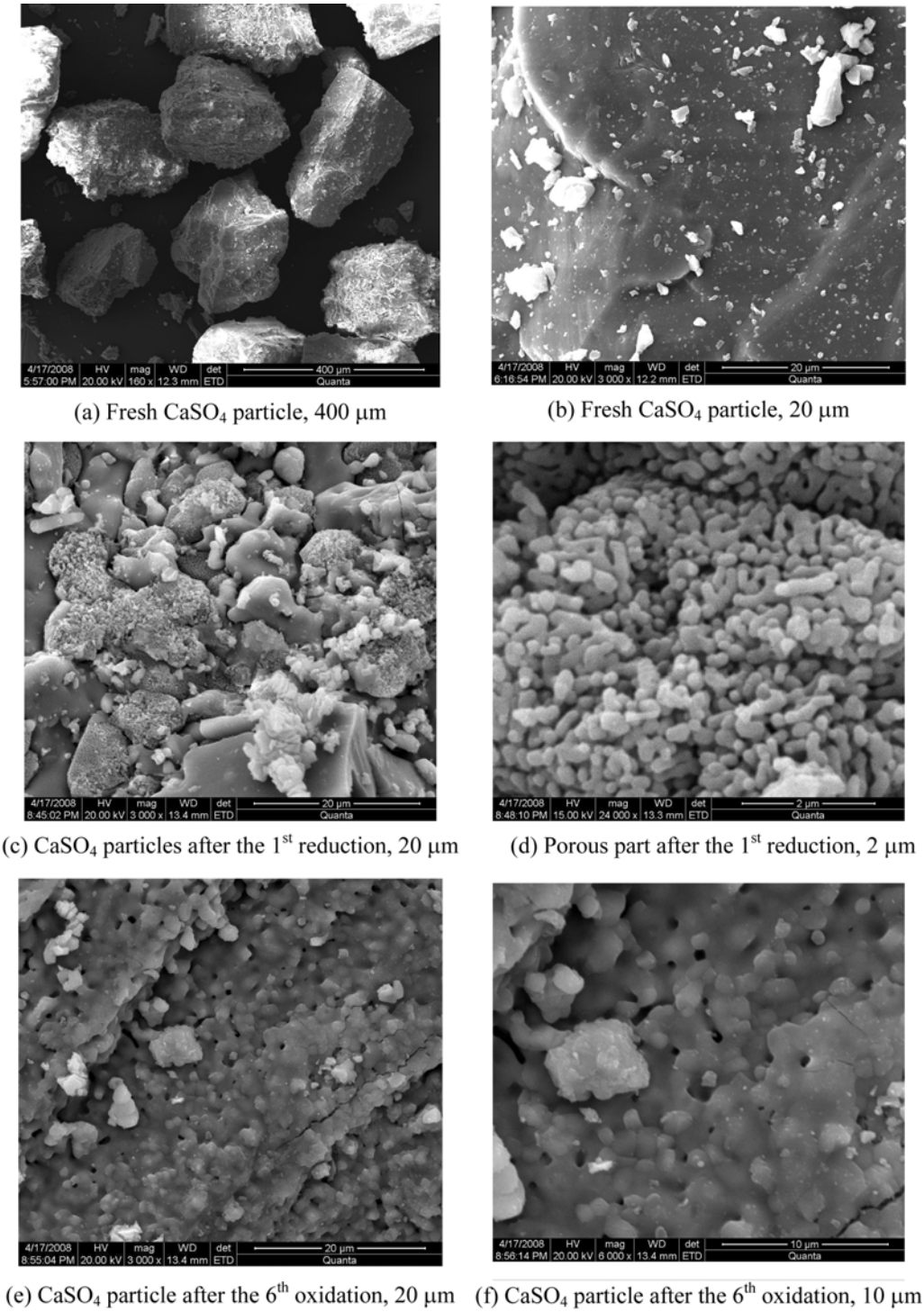

Fig. 10. SEM micrographs of the fresh and reacted oxygen carrier particles at typical temperatures.

unreacted $CaSO_4$. Since CaS is much more porous than $CaSO_4$ as observed from ESEM-EDS study, the porous product layer provides less resistance for the diffusion of CH_4 through the film surrounding the particles and the reaction can proceed further to the core. Therefore, the reduction and oxidation would mainly occur on the particle surface and chemical reaction could be the limiting mechanism that controls the reduction and oxidation process in this work. More work on kinetic study is needed to determine the reaction mechanisms.

CONCLUSIONS

In this study the reactivity of a $CaSO_4$ oxygen carrier in chemical-looping combustion of methane was conducted in a laboratory scale fixed bed reactor. The six-cycle test of $CaSO_4$ oxygen carrier in alternating reducing methane and oxidizing conditions was per-

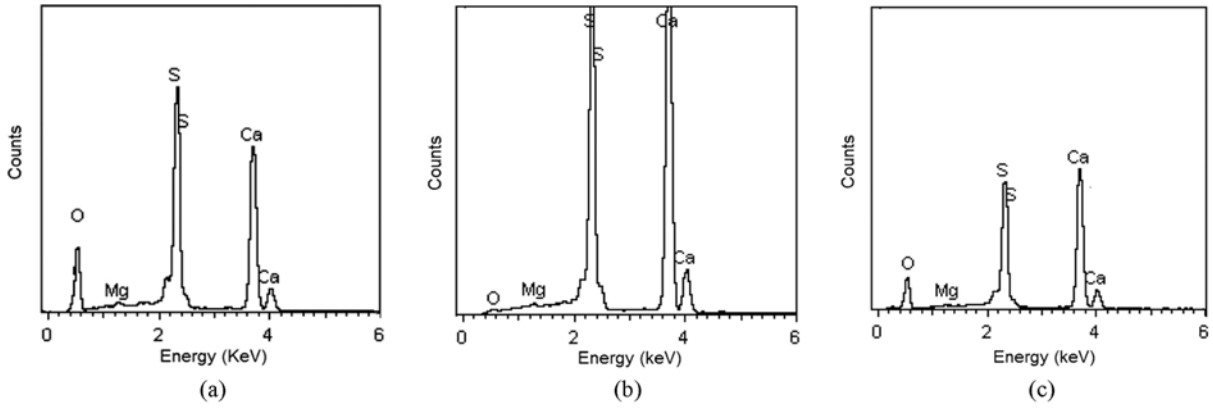

Fig. 11. Spectrums collected from the oxygen carrier particles for (a) fresh, (b) reduced after first cycle, and (c) used after 6^{th} oxidation.

Table 3. Atomic ratio of major elements on the surface of fresh and used $CaSO_4$ oxygen carrier particles

Species	Fresh sample	1^{st} reduction	6^{th} oxidation
S/Ca	1.146	1.0972	0.836
O/Ca	4.211	0.0026	3.635

formed to simulating the chemical-looping combustion. The main conclusions are as follows:

A majority of CH_4 reacted with $CaSO_4$ to form CO_2 and H_2O. The oxidation was incomplete and possibly could be ascribed to the $CaSO_4$ product layer in this study.

The CO_2 yield increased for the initial cycles but slightly decreased after four cycles. Carbon deposition during the reduction period was confirmed with the combustible gas ($CO+H_2$) in the product gas and slight CO_2 formed during the early stage of oxidation. The mechanism of carbon deposition and effect was also discussed.

The release of SO_2 during the cyclic test of reduction and oxidation verified the decrease of reactivity of $CaSO_4$ oxygen carrier in CLC. The possible SO_2 formation mechanism and mitigation method were discussed.

The oxygen carrier conversion after the reduction reaction decreased gradually in the cyclic test. The reactivity of $CaSO_4$ oxygen carrier increased for the initial cycles but slightly decreased after around four cycles due to the loss of sulfur and oxygen.

XRD analysis revealed that CaS was the main reduction product, while slight amount of CaO also formed in the cyclic test. ESEM analysis demonstrates the surface morphology variation from impervious for to porous after cyclic test. The particles tested in the fixed bed reactor were not uniform in porosity. EDS analysis provided the spectrum and average accurate quantitative analysis, which demonstrated the transfer of oxygen from $CaSO_4$ to fuel gas while leaving CaS as the dominant reduced product. The decrease of O/Ca and S/Ca atomic ratio on the surface was due to the loss of sulfur and oxygen in the form of SO_2.

The results show that $CaSO_4$ oxygen carrier may be an interesting candidate for oxygen carrier in CLC. There are also some technical problems such as low reactivity and sulfur release, that should be further studied.

ACKNOWLEDGMENT

The support from National Natural Science Foundation of China (Grant Nos. 50606006, 90610016) for this study is gratefully acknowledged.

NOMENCLATURE

dX_o/dt : oxidation rate of oxygen carrier [1/s]
dX_r/dt : reduction rate of oxygen carrier [1/s]
m : actual mass of oxygen carrier sample in the reactor [kg]
m_{ox} : mass of the sample when fully oxidized [kg]
m_{red} : mass of the sample in the reduced form [kg]
$\dot{n}_{in}$: molar flow of the gas entering the reactor [mol/s]
$\dot{n}_{out}$: molar flow of the gas exiting the reactor after water has been removed [mol/s]
n_o : amount of oxygen in oxygen carrier that can be removed from the fully oxidized oxygen carrier [mol]
R_o : oxygen transport capacity, or oxygen ratio of oxygen carrier, defined as $R_o=(m_{ox}-m_{red})/m_{ox}$
t : time [s]
T : temperature [°C]
X : oxygen carrier conversion, or the degree of oxidation
X_o : oxygen carrier conversion during oxidation reaction
X_r : oxygen carrier conversion during reduction reaction
$y_{i,in}$: inlet molar fraction of the gas species i entering the reactor
$y_{i,out}$: outlet molar fraction of the gas species i exiting the reactor after water removed

Greek Letters

ΔP : pressure difference [kPa]
ΔX : variation of the conversion of oxygen carrier
$\Delta\omega$: variation of the mass conversion of oxygen carrier
ω : mass based conversion of oxygen carrier
γ_i : gas yield of carbon species i in product gas [%]

Subscripts

in : inlet
out : outlet

REFERENCES

1. A. Lyngfelt, B. Leckner and T. Mattisson, *Chem. Eng. Sci.*, **56**, 3101

(2001).
2. M. Ishida and H. Jin, *Ind. Eng. Chem. Res.*, **35**, 2469 (1996).
3. H. G. Jin, T. Okamoto and M. Ishida, *Ind. Eng. Chem. Res.*, **38**, 126 (1999).
4. T. Mattisson, M. Johansson and A. Lyngfelt, *Energy Fuels*, **18**, 628 (2004).
5. P. Cho, T. Mattisson and A. Lyngfelt, *Fuel*, **83**, 1215 (2004).
6. M. Johansson, T. Mattisson and A. Lyngfelt, *Energy Fuels*, **20**, 2399 (2006).
7. T. Mattisson, M. Johansson and A. Lyngfelt, *Fuel*, **85**, 736 (2006).
8. J. Adánez, L. F. de Diego, F. García-Labiano, P. Gayán, A. Abad and J. M. Palacios, *Energy Fuels*, **18**, 371 (2004).
9. L. F. de Diego, F. García-Labiano, P. Gayán, J. Celaya, J. M. Palacios, and J. Adánez, *Fuel*, **86**, 1036 (2007).
10. B. M. Corbella, L. de Diego, F. García-Labiano, J. Adánez and J. M. Palacios, *Energy Fuels*, **20**, 148 (2006).
11. J. Adánez, P. Gayán, J. Celaya, L. F. de Diego, F. García-Labiano and A. Abad, *Ind. Eng. Chem. Res*., **45**, 6075 (2006).
12. H. J. Ryu, D. H. Bae and G. T. Jin, *Korean J. Chem. Eng.*, **20**, 960 (2003).
13. H. J. Ryu, D. H. Bae, K. H. Han, S. Y. Lee, G. T. Jin and J. H. Choi, *Korean J. Chem. Eng.*, **18**, 831 (2001).
14. H. J. Ryu and G. T. Jin, *Korean J. Chem. Eng.*, **24**, 527 (2007).
15. H. J. Ryu, N. Y. Lim, D. H. Bae and G. T. Jin, *Korean J. Chem. Eng.*, **20**, 157 (2003).
16. K. S. Song, Y. S. Seo, H. K. Yoon and S. J. Cho, *Korean J. Chem. Eng.*, **20**, 471 (2003).
17. S. R. Son and S. D. Kim, *Ind. Eng. Chem. Res.*, **45**, 2689 (2006).
18. L. H. Shen, M. Zheng, J. Xiao, H. Zhang and R. Xiao, *Sci. China Ser. E: Technol. Sci.*, **50**, 230 (2007).
19. L. Shen, M. Zheng, J. Xiao and R. Xiao, *Combust. Flame*, **154**, 489 (2008).
20. L. Shen, J. Wu and J. Xiao, *Combust. Flame*, **156**, 721 (2009).
21. T. Mattisson, A. Jardnas and A. Lyngfelt, *Energy Fuels*, **17**, 643 (2003).
22. H. E. J. Andrus, J. H. Chiu, P. T. Stromberg and P. R. Thibeault, in *22nd Annual international pittsburgh coal conference*, Pittsburgh, U.S.A. (2005).
23. J. S. Wang and E. J. Anthony, *Applied Energy*, **85**, 73 (2008).
24. E. J. Anthony, *Ind. Eng. Chem. Res.*, **47**, 1747 (2008).
25. Q. L. Song, R. Xiao, Z. Y. Deng, H. Y. Zhang, L. H. Shen and M. Y. Zhang, *Energy Conver. and Manage.*, **49**, 3178 (2008).
26. R. Xiao, L. H. Shen, M. Y. Zhang, B. S. Jin, Y. Q. Xiong, Y. F. Duan, Z. P. Zhong, H. C. Zhou, X. P. Chen and Y. J. Huang, *Korean J. Chem. Eng.*, **24**, 175 (2007).
27. R. Xiao, M. Y. Zhang, B. S. Jin, Y. J. Huang and H. C. Zhou, *Energy Fuels*, **20**, 715 (2006).
28. H. Zhou, B. Jin, Z. Zhong, Y. Huang, R. Xiao and Y. Zheng, *Korean J. Chem. Eng.*, **24**, 489 (2007).
29. G. Marbán, M. García-Calzada and A. B. Fuertes, *Chem. Eng. Sci.*, **54**, 77 (1999).
30. T. Mattisson, A. Lyngfelt and P. Cho, *Fuel*, **80**, 1953 (2001).
31. A. Abad, T. Mattisson, A. Lyngfelt and M. Johansson, *Fuel*, **86**, 1021 (2007).
32. L. F. de Diego, P. Gayán, F. García-Labiano, J. Celaya, M. Abad and J. Adánez, *Energy Fuels*, **19**, 1850 (2005).
33. K. Qiu, T. Mattisson, B. M. Steenari and O. Lindqvist, *Thermochim. Acta*, **298**, 87 (1997).
34. K. Qiu, O. Lindqvist and T. Mattisson, *Fuel*, **78**, 225 (1999).
35. P. Cho, T. Mattisson and A. Lyngfelt, *Ind. Eng. Chem. Res.*, **44**, 668 (2005).
36. P. Cho, T. Mattisson and A. Lyngfelt, *Ind. Eng. Chem. Res.*, **45**, 968 (2006).
37. M. Johansson, T. Mattisson, A. Lyngfelt and A. Abad, *Fuel*, **87**, 988 (2008).
38. H. Jin and M. Ishida, *Fuel*, **83**, 2411 (2004).
39. Q. L. Song, R. Xiao, Y. B. Li and L. H. Shen, *Ind. Eng. Chem. Res.*, **47**, 4349 (2008).
40. N. Berguerand and A. Lyngfelt, *Fuel*, **87**, 2713 (2008).
41. T. Mattisson and A. Lyngfelt, *Thermochim. Acta*, **325**, 59 (1999).
42. M. J. Fernandez, A. Lyngfelt and B. M. Steenari, *Energy Fuels*, **14**, 654 (2000).
43. H. Y. Sohn and B. S. Kim, *Ind. Eng. Chem. Res.*, **41**, 3081 (2002).
44. J. S. Dennis and A. N. Hayhurst, *Chem. Eng. Sci.*, **45**, 1175 (1990).
45. T. Mattisson and A. Lyngfelt, *Energy Fuels*, **12**, 905 (1998).
46. E. J. Anthony and D. L. Granatstein, *Prog. Energy Combust. Sci.*, **27**, 215 (2001).
47. M. Johansson, T. Mattisson and A. Lyngfelt, *Ind. Eng. Chem. Res.*, **43**, 6978 (2004).
48. N. H. Davies, K. M. Laughlin and A. N. Hayhurst, *Symposium (International) on Combustion*, **25**, 211 (1994).
49. N. H. Davies and A. N. Hayhurst, *Combust. Flame*, **106**, 359 (1996).
50. G. Marbán, M. García-Calzada and A. B. Fuertes, *Chem. Eng. Sci*., **54**, 495 (1999).